A Combined TEM and SAXS Study of the Growth and Self-Assembly of Ultrathin Pt Nanowires

Scott C. McGuire,[1] Yugang Zhang,[2] and Stanislaus S. Wong[1,*]

Email: stanislaus.wong@stonybrook.edu

[1]Department of Chemistry, State University of New York at Stony Brook,

Stony Brook, NY 11794-3400, USA

[2]Center for Functional Nanomaterials, Building 735,

Brookhaven National Laboratory,

Upton, NY 11973, USA

*To whom correspondence should be addressed.

Abstract

Ultrathin Pt nanowires possess high activity for various electrocatalytic applications. However, little work has focused on understanding their growth mechanisms. Herein, we utilize a combination of time-dependent, *ex situ* transmission electron microscopy (TEM) and small angle X-ray scattering (SAXS) techniques to observe the growth process in addition to associated surfactant-based interactions. TEM images indicate that initially nanoparticles are formed within 30 s; these small 'seed' particles quickly elongate to form ultrathin nanowires after 2 min. These motifs remain relatively unchanged in size and shape up to 480 min of reaction. Complementary SAXS data suggests that the initial nanoparticles, which are coated by a surfactant bilayer, arrange into a *bcc* superlattice. With increasing reaction time, the *bcc* lattice disappears as the nanoparticles grow into nanowires, which then self-assemble into a columnar hexagonal structure in which the individual nanowires are covered by a CTAB monolayer. The hexagonal structure eventually degrades, thereby leading to the formation of lamellar stacking phases comprised of surfactant bilayers. To the best of our knowledge, this is the first time that SAXS has been used to monitor the growth and self-assembly of Pt nanowires. These insights can be used to better understand and rationally control the formation of anisotropic motifs of other metallic nanostructures.

Introduction

Pt-based materials have been widely studied as electrocatalysts, due to their high intrinsic activity for a host of small-molecule reactions.[1-5] However, these catalysts suffer from a number of problems, including high production costs, stemming from the fact that Pt is both scarce and expensive. Moreover, Pt-based electrocatalysts often exhibit poor reaction kinetics and low stability, due to the presence of deleterious effects, such as the formation of partially oxidized products, dissolution, surface oxidation, and catalyst poisoning. As such, a considerable amount of work has focused on mitigating these deficiencies through various strategies, such as controlling either composition through alloying or morphology through the production of diverse structural motifs. One successful approach has focused on the synthesis of nanoscale formulations of Pt-based catalysts, which have been found to outperform their bulk counterparts, an observation ascribed in part to the relatively greater quantity of exposed, reactive surface sites, associated with nanostructures. In that context, research has centered on the fabrication of various Pt-based nanoscale analogues, such as but not limited to nanoparticles, nanocubes, nanoplates, nanocages, nanorods, and nanowires.[6-10]

Of this family of nanostructures, nanowires possess several unique advantages, especially those with average diameters in the ultrathin range (i.e., sub-10 nm).[6, 11, 12] In particular, the ultrathin motif allows for the exposure of proportionally more surface atoms and hence, more active sites for reactivity. In addition, the 1-dimensional (1D) structure enables stronger interactions with underlying supports, due to multiple points of physical and chemical contact with the support materials, all of which can inhibit particle detachment, therefore improving stability.[13, 14] Ultrathin nanowires also exhibit long, continuous, low-energy crystalline planes, which exhibit not only improved electronic transport properties but also a greater

resistance to Ostwald ripening.[15-18] Due to these advantages, ultrathin Pt nanowires have achieved superior performance for a variety of significant electrocatalytic reactions, such as but not limited to the oxygen reduction reaction (ORR), the hydrogen evolution reaction (HER), and the methanol oxidation reaction (MOR). Given the importance of this unusual architecture in catalysis, it has become increasingly significant and relevant to more precisely understand the nature of the intrinsic growth and control of the surface sites within this anisotropic nanowire motif with the goal of being able to determine structure-property correlations within this system.

The majority of prior work describing the growth process of ultrathin nanowires is based on *ex situ* transmission electron microscopy (TEM) experiments, wherein series of samples are generated under various controlled reaction conditions in order to determine the individual roles of different variables. Whereas this microscopy technique can provide for a considerable amount of useful insight into the growth process, there are also corresponding limitations to this methodology. For example, in preparing for standard TEM measurements, one often 'cleans' and 'washes' the sample to remove any excess reaction solution or surfactants; the powder is then dispersed in another solvent, prior to drop casting onto a TEM grid. As a result, the acquired images are not necessarily reflective of the various types of interactions that might be occurring within the reaction medium, as the nanowires are first nucleating and subsequently growing.

To mitigate for these issues, *in situ*, liquid-cell TEM (LCTEM) has been utilized to track the growth of various nanostructures in real time. As an illustrative example, Specifically, the technique has also been used to confirm that the growth of PtFe nanowires involved the initial formation of smaller nanoparticles which subsequently coalesced to form larger nanowire structures.[19, 20] While the ability to directly observe nanostructure growth is clearly a very useful tool, LCTEM also possesses a number of disadvantages, which limit the types of reactions

that it can be used to observe. Such limitations encompass not only the possibility of either chemical reduction or degradation of the reagents and subsequent products induced by the electron beam but also the physical geometric constraints associated with the LCTEM sample holder itself.[21, 22]

A complementary technique which is commonly used to track the growth and change in morphology of nanomaterials during a reaction process is small angle X-ray scattering (SAXS). Indeed, careful analysis of SAXS data can allow for the determination of particle shape, size, and number[23] of nanoparticles of varying chemical composition.[24] Indeed, this method has been used to monitor the formation of Pt nanoparticles under different reaction conditions; however, it has not as yet been applied to systematically probe the production of analogous Pt nanowires.[25, 26] In an effort that is similar but not identical to our work, one recent study focused on the effects of various reaction parameters, such as reaction temperature and time, on the growth of anisotropic Pt nanoparticles, possessing average aspect ratios of 1.3.[27] It was determined that the length was not significantly affected by the heating protocol employed, whereas the radius was increased by decreasing both the reaction temperature and heating rate.

It should be noted that in this previous study, 1D Pt nanostructures were generated during *ex situ* measurements. However, only nanoparticles were generated under their reported *in situ* SAXS measurements. This difference in observed particle shape might have been due to the reduction of the Pt precursor via X-ray irradiation as opposed to any chemical means, a possible scenario which has been previously reported[28] and which would have altered the expected growth mechanism. As such, while the synthesis method used herein is similar to what has been done in this prior study, by contrast, herein we embarked upon a series of time-dependent *ex situ* SAXS measurements to monitor the growth of Pt nanowires to mitigate and prevent the influence

and potentially deleterious, interfering effects of X-rays on the observed growth mechanism. Moreover, this approach has also allowed us to bear witness to the self-assembly of smaller constituent units into the nanowires themselves, which has not been previously reported for 1D Pt nanostructures.

It should be indicated that while no papers to date have focused on using SAXS to characterize the production of Pt nanowires, related publications have reported on the growth of analogous ultrathin Au nanowires.[29-34] Moreover, SAXS has also been used to characterize a large number of superstructures,[35-39] wherein nanostructures act as building blocks that self-assembled into an ordered structure. The formation of superstructures can lead to the emergence of distinctive peaks, whose relative peak positions can be used to solve for the lattice parameters of the as-formed superstructures, thereby allowing for the determination of variables such as the interparticle distance. Coupled with additional information such as the known length of the surfactants, these computed distance measurements can be used to identify how the ligands were able to arrange and pack onto the surface.

Specifically, SAXS has been used to determine if self-assembly occurred during the reaction process of Au nanowires.[40] In fact, it was deduced that Au nanowires could arrange themselves into a hexagonal close packed (*hcp*) arrangement; the lattice parameter of the resulting superstructure was calculated to be 9.7 nm. By subtracting off the observed diameter of the nanowires (1.7 nm), an interwire distance of 8 nm was computed. This value is roughly four times the length of oleylamine, the surfactant utilized in the reaction, implying that the individual nanowires were likely coated with a bilayer of oleylamine.[29] In a similar study, wherein oleylamine was utilized as a surfactant within a cyclohexane solution, it was determined that ultrathin Au nanowires, characterized by individual diameters of 1.6 – 1.7 nm, could self-

assemble into a *hcp* arrangement, with an average 'center-to-center' wire distance of 5.9 nm, a value which is consistent with the generation of a monolayer of oleylamine ligands on the outer surface of the wires.[33] In effect, it was determined that the actual reactions conditions used, including the concentration of surfactants, had a direct and notable effect on the ability of nanowires to undergo self-assembly. We make use of similar types of analysis and calculations in the work we present herein.

Moreover, DFT calculations have suggested a cooperative adsorption and organization of ion pairs at the surfaces of these ultrathin Au nanowires, implying the key role of the charged backbone in the growth of these anisotropic motifs.[30] Finally, in terms of relevant precedence, synchrotron-based grazing-incidence SAXS has been used to track the aggregation and real-time, interfacial assembly (under Langmuir-Blodgett conditions) of randomly dispersed Te and Ag nanowires into ordered nanowire blocks and ultimately, well-defined nanowire monolayers, driven by conformational entropy considerations.[41]

The goal of this work was therefore to examine and follow the growth of Pt nanowires, synthesized during a wet chemical synthesis protocol, using a combination of *ex situ* TEM and SAXS measurements. While we concluded that the growth process of the ultrathin nanowires likely occurs in a very small time frame (less than 1 min), it was observed that the nanowires interacted with not only the surfactants but also the reaction solution itself in order to yield superstructures, which evolved over time. This formation and evolution of superstructures, comprised of individual Pt nanowires, to the best of our knowledge, has not as yet been reported. Hence, understanding the growth process (and accompanying factors, such as the role of surfactant interactions within it) will be crucial towards developing rational and predictive control over the morphology and composition of these ultrathin nanostructures.

Experimental

Materials: Oleylamine (OAm, 70%, Sigma Aldrich), hexadecyltrimethylammonium bromide (CTAB, ≥98%, Sigma Aldrich), molybdenum hexacarbonyl ($Mo(CO)_6$, Alfa Inorganics), potassium bromide (KBr, Certified ACS, Fisher), and platinum acetylacetonate ($Pt(acac)_2$, 98%, Acros Organics) were purchased from their respective sources.

Synthesis of Pt NWs: The protocol that we focused on herein was adapted from a previously reported procedure.[42] To create these ultrathin nanowires, within a vial, 10 mg $Pt(acac)_2$, 32 mg CTAB, and 10 mg $Mo(CO)_6$ were dispersed in 4 mL of oleylamine and sonicated for 30 min. Subsequently, the capped vial was placed into an oil bath, which had been pre-heated to 180°C, and it was left to react for 0.5 to 480 min without any stirring whatsoever. The reaction was then quenched by removing the vial from the oil bath and placing it into a water bath.

Characterization:

Transmission electron microscopy: TEM images were acquired using a JEOL-1400 microscope, operated at an acceleration voltage of 120 kV. High resolution TEM (HRTEM) images were obtained with a JEOL 2100F microscope, run at an acceleration voltage of 200 kV. Samples were prepared by drop-casting aliquots onto lacey carbon grids.

Small angle X-ray scattering: Aliquots of the prepared reaction solutions were transferred to quartz capillaries, possessing a diameter of 1.0 mm and a wall thickness of 0.01 mm (Charles Supper). The small-angle X-ray scattering (SAXS) measurements were conducted at the Soft Matter Interfaces beamline (12-ID) of the National Synchrotron Light Source II (NSLS-II) at Brookhaven National Laboratory. The scattered data were collected using a beam energy of 16.1 keV and a beam size of 200 X 30 um with a Pilatus 1M area detector (Dectris, Switzerland). The detector, consisting of 0.172 mm square pixels in a 981 X 1043 array, was physically placed two

meters downstream from the sample position. The collected 2D scattering patterns were reduced to a 1D scattering intensity, I(q), by circular averaging. The q denotes a wave vector transfer in which $q = (4\pi/\lambda) \sin(\theta)$, wherein $\lambda = 0.77$ Å and 2θ represents the wavelength of the incident x-ray beam and the scattering angle, respectively.

Results and Discussion

To generate the desired Pt nanowires, we have used a reliable, previously reported synthesis method. This procedure has been strategically chosen, due to its simplicity and ability to generate uniform, relatively straight ultrathin nanowires. The production of uniform, well defined structures is important, because it simplifies characterization by SAXS. Specifically, $Pt(acac)_2$ was reacted in the presence of oleylamine, hexadecyltrimethylammonium bromide (CTAB), and $Mo(CO)_6$ at 180°C for 480 min. The role of oleylamine is not only as the underlying reaction medium but also as a participatory surfactant. CTAB functions as an additional surfactant, while $Mo(CO)_6$ acts as both a reducing agent and a structure-directing agent.[42-45] In order to test and determine the importance of each individual reactant, we also ran a separate series of independent experiments in which each specific reagent was selectively removed from the reaction vessel, all else being equal.

TEM images of the various different samples are shown in **Figure 1**. These data indicate that under typical reaction conditions, ultrathin nanowires are formed with average, measured diameters of 1.6 ± 0.3 nm. Not surprisingly, when no Pt precursor is added to the reaction solution, no solid product is formed. In the absence of CTAB, only spherical nanoparticles with average diameters of 5.0 ± 0.4 nm are isolated. Similarly, when CTAB is replaced with KBr, an identical outcome was observed, namely the generation of spherical particles with average

diameters of 5.0 ± 0.4 nm. These findings suggest that the presence of CTAB is essential to the formation of anisotropic 1D nanostructures, while conversely, Br^- ions do not significantly impact upon the observed morphology. Interestingly, when the reaction is conducted in the absence of $Mo(CO)_6$, a mixture of nanoparticles and multi-podal nanostructures, characterized by average diameters of 11 ± 1 nm, was observed. This result suggests that $Mo(CO)_6$ likely behaves as an additional structure-directing agent with which to enable the anisotropic growth of the as-generated nanowires; one mechanism with which this might occur involves the in situ formation of CO.[46, 47] Representative HRTEM images of each of the different samples produced under these diverse sets of reaction conditions (Figure S1) are consistent with the presence of a Pt(111) plane, characterized by a *d*-spacing of 0.23 nm, as expected.

To gain insights into the growth mechanism, we first ran experiments forming Pt nanowires and removed aliquots of products at different, discrete reaction times. TEM images of the resulting products at each specific time stage are shown in **Figure S2**. After a reaction time of 0.5 min, the product consisted of anisotropic nanoparticles, characterized by average diameters of 2.4 ± 0.9 nm and aspect ratios of 2.8 ± 1.9. Increasing the reaction time to 1 min yielded ultrathin nanowires, possessing diameters of 1.6 ± 0.4 nm coupled with a more polydisperse range of associated aspect ratios of 6.7 ± 5.1. Boosting the reaction time still further had little effect on the measured diameter of the nanowires. Lengths increased as one would have expected, although the observed aspect ratio remained between 10 and 20. It should be noted that the samples formed at a relatively shorter reaction time (i.e., less than 5 min) contained not only a large proportion of nanowires but also a higher fraction of nanoparticles than was subsequently isolated after comparatively longer reaction times.

These results are similar to what had been recorded by another group working on Rh-doped Pt nanowires, which had been synthesized using a similar didecyldimethylammonium bromide (DDAB) surfactant. In that study, it was postulated that the surfactants self-organized into a reverse micelle structure framework, onto which the metallic particles subsequently formed.[42] In addition, the surfactants likely exhibited a lower packing density at the ends of the particles, thereby allowing for the metals to be chemically reduced and subsequently deposited preferentially along their longitudinal axis in order to generate the resulting nanowires. Indeed, we expect that a similar mechanism takes place in the synthesis described herein in this work, with CTAB substituting for DDAB. Therefore, we have conducted a series of SAXS measurements to further probe and understand the growth mechanism of these nanowires.

First, we compared the SAXS results of the samples generated under different precursor and reaction conditions, albeit at the same reaction time of 480 min to determine if there were any clear and noticeable differences in this set of spectra. To this end, **Figure 2** compares the SAXS spectra corresponding to the samples generated (i) without Pt, (ii) without CTAB, (iii) with KBr, (iv) without $Mo(CO)_6$, and (v) under typical reaction conditions (i.e., in the presence of CTAB), respectively. Each spectrum yielded peaks which appear at higher values of q, a phenomenon which can be ascribed to the formation of superstructures. Spectra for the samples generated either without CTAB or with KBr were quite similar, an observation which is understandable, given the near-identical morphologies isolated after these runs, as determined by TEM. Interestingly, all of the other samples exhibited unique sets of identifiable features. These data suggest that changing the composition and concentration of reactants and surfactants gives rise to a significant and perceptible effect upon the as-growing nanowire environment. In effect,

we can ascribe the peak and profile differences within these different spectra to chemically dissimilar and distinctive molecular interactions with the ever-evolving metal nanowire surface.

Second, to investigate and track the evolution of nanowire-surfactant interactions as a function of time, we conducted a series of SAXS measurements on samples generated at various reaction times, with all other reaction parameters kept constant. **Figure 3A** displays the SAXS spectra of samples generated within the first 2 min of reaction. All of these spectra exhibited a peak, centered at 0.118 $Å^{-1}$. This same peak was observed in spectra associated with a sample which had not been exposed to any heating whatsoever, i.e., where no reaction was presumed to have occurred. As such, it is likely that this peak arises from interactions between the precursors and the reaction medium. For example, the SAXS spectra of OAm alone, in the absence of any heating, gave rise to a single peak located at 0.125 $Å^{-1}$. A similar peak feature, situated at 0.128 $Å^{-1}$, was observed in the 0.5 min sample. It subsequently decreased in intensity and shifted ever so slightly to 0.125 $Å^{-1}$ after 2 min of reaction. We can reasonably attribute this peak to the presence of OAm in its role as both the solvent and the participatory surfactant.

Additional features, located at 0.083, 0.166, and 0.249 $Å^{-1}$ within the 0.5 min sample, decreased in intensity with increasing reaction time and were no longer visible after 2 min. The expected peak positions for a *bcc* superlattice were calculated and are shown as red dashed lines in **Figure 3A**. While not all of the expected *bcc* peaks are observed, the peaks centered at 0.083, 0.166, and 0.249 $Å^{-1}$ line up reasonably well with what would be expected for the (110), (220), and (411) planes of that crystal lattice, respectively. The lack of any remaining identifying peaks, associated with the superlattice, may have been due to issues such as but not limited to (i) low intensities, (ii) the presence of additional, overlapping features from other surfactants, and (iii)

the poor overall uniformity of the superlattices, as evidenced by the broadened intrinsic nature of the (110), (220), and (411) peaks.

The lattice parameter, *a*, is calculated using Equation 1, in which *h*, *k*, and *l* are the Miller indices, yielding a value of 10.7 nm. The edge length, *x*, of a *bcc* unit cell is defined by Equation 2, wherein '*r'* is the radius of the nanoparticles. When using the calculated *a* value of 10.7 nm as '*x'*, *r* is determined to be 4.6 nm, which is almost twice the particle size that was experimentally measured using TEM analysis (i.e., 1.9 nm).

$$q = 2\pi\sqrt{\frac{h^2 + k^2 + l^2}{a^2}}$$

(Equation 1)

$$x = \frac{4}{\sqrt{3}}r$$

(Equation 2)

This discrepancy suggests that the particles are likely coated with a surfactant shell, computed to have a thickness of about 3.6 nm. This dimension is similar to and consistent with the length reported for an oleylamine bilayer. However, it has been previously reported under similar reaction conditions that CTAB and oleylamine are both bound onto the surface of Pt, thereby suggesting that the surfactant bilayer observed herein likely consists of both CTAB and oleylamine. Therefore, it seems that within the early stages of the synthesis, Pt nanoparticles are initially formed and subsequently enclosed within an oleylamine / CTAB bilayer 'shell', which arranges itself as a *bcc* superlattice. As reaction time increases, the length of the individual nanoparticles presumably correspondingly increases, a consequence of which is that the initial surfactant-based *bcc* superlattice disappears over time.

Indeed, **Figure 3B** highlights the spectra for samples generated between reaction times of 2 to 30 min. Specifically, increasing the time beyond 2 min led to a significant alteration in the observed features. Though the peak, ascribed to oleylamine and located at 0.125 $Å^{-1}$, increased in intensity after 2 min of reaction, it remained essentially unchanged up to 30 min. Conversely, two newer and broader peaks began to form after 5 min; these were positioned at 0.148 and 0.256 $Å^{-1}$, and could be indexed to a columnar hexagonal structure. Moreover, as the reaction time was increased, these peaks correspondingly rose in intensity but downshifted to values of 0.133 and 0.231 $Å^{-1}$, respectively.

The lattice parameter for a columnar hexagonal structure is defined by Equation 3, which is also equivalent to the 'center-to-center' wire distance. Assigning the values of the positions of the first peaks for the 5- and 30-min samples as q_{5min} and q_{30min}, we calculated associated a values of 4.2 and 4.7 nm, respectively.

$$q = 2\pi\sqrt{\frac{h^2 + hk + k^2}{a^2}}$$

(Equation 3)

It is worth pointing out that interwire distances as large as 8 nm have been reported for ultrathin Au nanowires, in which stabilization was provided by the ligand's double layer composed to oleylamine and oleylammonium chloride.[31] Moreover, it has also been reported that ultrathin Au ultrathin nanowires arranged in a *hcp* structure appear to be stabilized within a monolayer of oleylamine, achieving 'center-to-center' distances of ~5.5 and 4.1 nm, when using alkanes and alcohols as solvents, respectively.[48] This clear difference in distances observed between alkanes and alcohols can be caused by the occurrence of interdigitation (and similar types of bonding interactions) within alcohols, whereas little to no interdigitation occurs within alkane

solvents. This finding highlights that varying reaction conditions can lead to a difference in surfactant interactions and thereby impact observed interparticle distances.

By subtracting off the observed nanowire diameter as measured by TEM (i.e., 1.5 nm) at these time points, the distance between nanowires for the 5- and 30-min samples were determined to be 2.7 and 3.2 nm, respectively. In other words, our data imply that there is a monolayer of excess CTAB surfactant molecules surrounding the growing nanowires,[34, 49] which expands in size with increasing reaction time, possibly due to a reduction in the amount of interdigitation and analogous intermolecular interactions. Indeed, a similar type of hexagonal structure has been observed by SAXS in ultrathin Au nanowire systems, which were found to have been capped by a bilayer of oleylamine.[31]

At 15 min of reaction, an additional peak feature centered at 0.197 $Å^{-1}$ began to appear, and it heightened in intensity at 30 min. Interestingly, this peak location is identical to that observed in the sample synthesized in the absence of any Pt whatsoever. Hence, it is unlikely that this peak can be associated with Pt itself; rather, it might be ascribed to unrelated phenomena, such as but not limited to surfactant-solvent interactions.

Increasing the reaction time beyond 30 min led to a perceptible decrease in and eventual disappearance of the set of peaks, that we had previously ascribed to the columnar hexagonal structure, as shown in **Figure 3C**. Furthermore, the extraneous peak at 0.197 $Å^{-1}$ of unknown origin (previously mentioned) appeared to have strengthened in intensity after 45 min but then diminished at 60 min, coincident with the incipient formation of a new peak at 0.190 $Å^{-1}$. We should note that this new peak occurs at the same position as what was observed in the sample synthesized in the absence of $Mo(CO)_6$. Again, it is unlikely that this peak originates from any self-assembly process, since it is unlikely that non-uniform nanostructures, generated without

any $Mo(CO)_6$ present whatsoever, can arrange into an ordered structure. As such, by analogy to the peak observed at 0.197 $Å^{-1}$, we can likely assign this emerging signal to phenomena, unrelated to the growth process, including the presence of surfactant-solvent interactions. Increasing the reaction time further to 120 min and beyond, as shown in **Figure 3D**, led to an increase in the peak intensity of the signal localized at 0.190 $Å^{-1}$. Indeed, it remained essentially invariant to 240 min, and after 480 min, almost completely disappeared, though was still present.

In addition, at 120 min, we observed not only a peak located at 0.121 $Å^{-1}$, referred to as q_1, which is similar to the peak in all previous samples that had been attributed to oleylamine but also an additional peak situated at 0.242 $Å^{-1}$, equivalent to $2q_1$. These two peaks taken together could be collectively attributed to the (001) and (002) planes of a lamellar stacking phase. Moreover, at this 120 min time point, we detected the presence of an additional lamellar stacking phase characterized by peaks positioned at 0.135 and 0.270 $Å^{-1}$, corresponding to the (001) and (002) planes, respectively. Using Equation 4, wherein '*c'* is the lattice parameter for the lamellar stacking phase, it was determined that the distance between the layers was 5.2 nm.

$$q_1 = 2\pi\sqrt{\frac{l^2}{c^2}}$$

(Equation 4)

Subtracting off the average diameter of these as-prepared nanowires, as measured by TEM to be 1.7 nm, we postulate that a surfactant layer with a thickness of 3.6 nm was present at this stage, similar to dimension to what had been previously reported for analogous bilayers of oleylamine.[50, 51] Moreover, by calculating the associated lattice parameter for the second lamellar phase, '*c'* was estimated to be 4.6 nm, thereby yielding a surfactant layer thickness of 2.9 nm, which was similar in magnitude to what had been previously reported for CTAB

bilayers. We found that the peaks related to the larger lamellar phase essentially disappeared with increasing reaction time beyond 120 min. By contrast, the peaks associated with the smaller lamellar phase rose in intensity and shifted slightly to lower values past 120 min; our calculations yielded a bilayer thickness quantity of 2.8 nm. Indeed, after 480 min of reaction, the CTAB-induced lamellar stacking phase became the pre-dominant structure observed by SAXS. For the sake of completeness, it should be noted that after 480 min, a new but unidentified peak was observed, located at 0.162 $Å^{-1}$.

In summary, the synthesis of ultrathin Pt nanowires can be summarized as occurring within the context of four well-defined stages, a process illustrated in Figure 4. The first stage (seconds to a few min) occurs at the very initiation of the reaction process itself, wherein Pt nanoparticles are immediately formed; these nanoparticulate species are capped by a surfactant monolayer, arrange into a *bcc* superlattice **(Figure 4A)**, and subsequently grow into nanowire-like motifs. In the second stage occurring after 5 min, the nanowires assemble into a columnar hexagonal structure, characterized by an interwire distance of 2.7 nm, that can be attributed to a surfactant monolayer coating each of the nanowires. The distance between the nanowires increases to 3.2 nm upon a rise in reaction time to 30 min **(Figure 4B)**. The third stage begins after 30 min, wherein the columnar hexagonal structure begins to break down. There is no apparent self-assembly process occurring from 45 min until 120 min. The final step consists of the formation of two lamellar phases at 120 min; we have hypothesized herein that these are comprised of surfactant bilayers with thicknesses of 3.6 and 2.9 nm, which can be reasonably ascribed to oleylamine and CTAB, respectively. Increasing the reaction time still further to 240 and 480 min led to the disappearance of the oleylamine bilayer, whereas the remaining CTAB bilayer contracted slightly to 2.8 nm **(Figure 4C)**. Overall, these results indicate that while the

desired ultrathin nanowire structure is likely already formed within the first 10 min of reaction, the interactions of these wires with the surrounding surfactant molecules within the reaction environment continue to evolve and change for a far longer period of time than has been previously reported and discussed in the literature. In effect, we have observed that local surfactant structure and degree of packing will alter over considerably extended periods (up to and beyond 480 min), with unexplored implications for the type, density, and orientation of additional ligands that can be reasonably attached onto these metal nanowire surfaces.

By means of comparison, we have also conducted time-dependent TEM and SAXS measurements **(Figures S3 and S4)** for nanoparticles synthesized in the presence of a non-surfactant species, namely KBr, as opposed to CTAB, with all other reaction parameters kept constant. **Figure S3** displays the TEM images of nanoparticles synthesized with reaction times of 1, 5, 45, 120, and 480 min, respectively. The 1 min sample gave rise to nanoparticles with average sizes of 3.0 ± 0.4 nm, whereas all of the other isolated samples yielded sizes of about 5 nm. These data collectively indicate that the maximum size of nanoparticles that can be generated under these reaction conditions is ~5 nm and that these nanoparticles can be produced within 5 min of reaction time. From the SAXS data shown in **Figure S4**, after 1 min, there are barely any features present, except for a small peak centered at 0.126 $Å^{-1}$, which can be attributed to oleylamine. With increasing reaction times, more features become apparent with the sample at 45 min evincing the most well-defined peaks. It should be noted that the observed differences in intensities between the various samples may be due to sample concentration.

The various peaks within the 45 min sample can be indexed to a *bcc* superlattice, characterized by a lattice parameter of 11.0 nm. Using the nanoparticle size dimension determined by TEM at 45 min (i.e., $d \approx 5$ nm), as per our previous calculations, it was deduced

that the particles are likely capped by a 2.2 nm thick surfactant layer. This layer is smaller than what had been observed for the particles synthesized at 1 min with CTAB. As such, we postulate that the nanoparticles may be covered with a monolayer of oleylamine. In effect, with this idea in mind in addition to the outcomes of the rest of our reported experiments herein, we hypothesize that CTAB and oleylamine essentially compete with each other in coating the individual Pt nanoscale building blocks. That is, in the presence of CTAB, enveloping and surrounding Pt nanoparticles, these can attach and grow in an anisotropic manner to form 1D structures. Conversely, when Pt nanoparticles are synthesized in the absence CTAB, they are instead coated with oleylamine, which likely uniformly covers the outer nanoparticle surface, thereby inhibiting particle-particle interactions and possible anisotropic growth.

Conclusions

It has been proposed that the metal atoms of ultrathin Au nanowires assemble in a way so as to maximize atomic packing density while keeping atomic-level stresses low, thereby favoring the production of cylindrical motifs characterized by well-defined diameters and atomically smooth surfaces.[52] We have utilized a combination of TEM and SAXS measurements to probe the growth and subsequent formation of ultrathin Pt nanowires, emphasizing the key role of surfactant interactions in enabling this process. By TEM, it was observed that constituent particles are formed essentially immediately (within 30 s), which then elongate into nanowires within 2 min and then remain relatively unchanged up to 480 min. This behavior is analogous to the ‘coalescence’ mechanism reported for pure and alloyed nanoparticles.[24] What is more intriguing is that the SAXS data suggest that the nanoparticles created at the very beginning of the reaction are initially coated by a bilayer of oleylamine / CTAB which had self-assembled into

a *bcc* superlattice. As the nanoparticles subsequently assemble and grow into nanowires, the *bcc* lattice disappears, and the nanowires begin to arrange into a columnar hexagonal structure in which the constituent nanowires are coated with a monolayer of CTAB ligands. After additional reaction time, the columnar structure starts to degrade, and then two lamellar phases arise. These have been attributed to individual bilayers of both oleylamine and CTAB. After 480 min of reaction time, the oleylamine bilayer is no longer present, and the nanowires are enclosed and sandwiched between the outer CTAB bilayers.

To the best of our knowledge, this is the first time that SAXS has been used to characterize the surfactant interactions impacting the growth and formation of ultrathin Pt nanowires during their synthesis. It is worth pointing out that variables, including precursor concentration, temperature, the presence of stabilizing ligands, and co-solvents are all known to impact upon the temporal evolution of as-generated particle sizes and size distributions.[53] For example, differences in ligand mobility and the rate of capping onto various facet types can favor the preferential growth of one shape (e.g., cubes versus spheres versus octahedra) as opposed to another.[54-56] These molecular-level insights can be used to better understand and control the formation, evolution, and development of not only ultrathin metal nanowires in particular but also nanowires of arbitrary composition in general, in the presence of additives such as but not limited to surfactants. Future work will focus on in situ SAXS, as the technique has been used to provide additional clarity into nanoscale organization;[40] for example, the structure of supercrystalline lattices derived from Au nanoparticles is governed by both the liquid-liquid interface and interparticle Lennard-Jones-like potentials.

Acknowledgements

This material is based on work supported by the U.S. National Science Foundation under Grant No. CHE-1807640. Electron microscopy studies for this manuscript were performed in part at the Center for Functional Nanomaterials (CFN), an Office of Science facility located at Brookhaven National Laboratory (BNL), which is supported by the U.S. Department of Energy under Contract No. DE-SC0012704. This research also used resources of the CFN and the SMI beamline (12-ID) of the National Synchrotron Light Source II, both supported by the U.S. Department of Energy Office of Science Facilities at BNL under Contract No. DE-SC0012704.

References

1. Ren, X.; Lv, Q.; Liu, L.; Liu, B.; Wang, Y.; Liu, A.; Wu, G., 2020 *Sustain. Energy Fuels* ***4*** 15-30.
2. Mahata, A.; Nair, A. S.; Pathak, B., 2019 *Catal. Sci. Technol.* ***9*** 4835-4863.
3. Li, C.; Baek, J.-B., 2020 *ACS Omega* ***5*** 31-40.
4. Kim, J. M.; Kim, J.-H.; Kim, J.; Lim, Y.; Kim, Y.; Alam, A.; Lee, J.; Ju, H.; Ham, H. C.; Kim, J. Y., 2020 *Adv. Mater.* ***32*** 2002210.
5. Eftekhari, A., 2017 *Int. J. Hydrogen Energy* ***42*** 11053-11077.
6. Lai, J.; Guo, S., 2017 *Small* ***13*** n/a.
7. Quinson, J.; Jensen, K. M. O., 2020 *Adv. Colloid Interface Sci.* ***286*** 102300.
8. Liu, M.; Zhao, Z.; Duan, X.; Huang, Y., 2019 *Adv. Mater.* ***31*** n/a.
9. Ding, H.; Wang, S.; Long, Y.; Chan, S. H., 2021 *Mater. Today Energy* ***19*** 100616.
10. Chen, A.; Holt-Hindle, P., 2010 *Chem. Rev.* ***110*** 3767-3804.
11. Wang, Y.; Yuan, Y.; Huang, H., 2021 *Chin. J. Chem.* ***39*** 1389-1396.
12. Li, L.; Wong, S. S., 2018 *ACS Omega* ***3*** 3294-3313.
13. Li, M.; Zhao, Z.; Cheng, T.; Fortunelli, A.; Chen, C.-Y.; Yu, R.; Zhang, Q.; Gu, L.; Merinov, B. V.; Lin, Z.; Zhu, E.; Yu, T.; Jia, Q.; Guo, J.; Zhang, L.; Goddard, W. A., III; Huang, Y.; Duan, X., 2016 *Science* ***354*** 1414-1419.
14. Luo, M.; Sun, Y.; Zhang, X.; Qin, Y.; Li, M.; Li, Y.; Li, C.; Yang, Y.; Wang, L.; Gao, P.; Lu, G.; Guo, S., 2018 *Adv. Mater.* ***30*** 1705515.
15. Sun, S.; Zhang, G.; Geng, D.; Chen, Y.; Li, R.; Cai, M.; Sun, X., 2011 *Angew. Chem., Int. Ed.* ***50*** 422-426, S422/1-S422/5.
16. Jiang, K.; Bu, L.; Wang, P.; Guo, S.; Huang, X., 2015 *ACS Appl. Mater. Interfaces* ***7*** 15061-15067.
17. Huang, H.; Ruditskiy, A.; Choi, S.-I.; Zhang, L.; Liu, J.; Ye, Z.; Xia, Y., 2017 *ACS Appl. Mater. Interfaces* ***9*** 31203-31212.
18. Guo, S.; Li, D.; Zhu, H.; Zhang, S.; Markovic, N. M.; Stamenkovic, V. R.; Sun, S., 2013 *Angew. Chem., Int. Ed.* ***52*** 3465-3468.
19. Liao, H.-G.; Zheng, H., 2013 *J. Am. Chem. Soc.* ***135*** 5038-5043.
20. Liao, H.-G.; Cui, L.; Whitelam, S.; Zheng, H., 2012 *Science* ***336*** 1011- 1014.
21. Sun, Y.; Ren, Y., 2013 *Part. Part. Syst. Charact.* ***30*** 399-419.
22. Hodnik, N.; Dehm, G.; Mayrhofer, K. J. J., 2016 *Acc. Chem. Res.* ***49*** 2015-2022.
23. Li, T.; Senesi, A. J.; Lee, B., 2016 *Chem. Rev.* ***116*** 11128-11180.
24. Garcia, P. R. A. F.; Prymak, O.; Grasmik, V.; Pappert, K.; Wlysses, W.; Otubo, L.; Epple, M.; Oliveira, C. L. P., 2020 *Nanoscale Adv.* ***2*** 225–238.
25. Wang, W.; Chen, X.; Cai, Q.; Mo, G.; Jiang, L. S.; Zhang, K.; Chen, Z. J.; Wu, Z. H.; Pan, W., 2008 *Eur. Phys. J. B* ***65*** 57-64.
26. Steinfeldt, N., 2012 *Langmuir* ***28*** 13072-13079.
27. Yoshimune, W.; Kuwaki, A.; Kusano, T.; Matsunaga, T.; Nakamura, H., 2021 *ACS Omega* ***6*** 10866-10874.
28. Wang, C.-L.; Hsao, B.-J.; Lai, S.-F.; Chen, W.-C.; Chen, H.-H.; Chen, Y.-Y.; Chien, C.-C.; Cai, X.; Kempson, I. M.; Hwu, Y.; Margaritondo, G., 2011 *Nanotechnology* ***22*** 065605.

29. Pschunder, F.; Puig, J.; Giovanetti, L. J.; Huck-Iriart, C.; Requejo, F. G.; Buceta, D.; Hoppe, C. E.; Ramallo-Lopez, J. M., 2018 *J. Phys. Chem. C* ***122*** 29051-29061.
30. Loubat, A.; Lacroix, L.-M.; Robert, A.; Imperor-Clerc, M.; Poteau, R.; Maron, L.; Arenal, R.; Pansu, B.; Viau, G., 2015 *J. Phys. Chem. C* ***119*** 4422-4430.
31. Loubat, A.; Imperor-Clerc, M.; Pansu, B.; Meneau, F.; Raquet, B.; Viau, G.; Lacroix, L.-M., 2014 *Langmuir* ***30*** 4005-4012.
32. Liang, Y.; Xie, Y.; Chen, D.; Guo, C.; Hou, S.; Wen, T.; Yang, F.; Deng, K.; Wu, X.; Smalyukh, I. I.; Liu, Q., 2017 *Nat. Commun.* ***8*** 1-8.
33. Bettscheider, S.; Kuttich, B.; Engel, L. F.; Gonzalez-Garcia, L.; Kraus, T., 2021 *J. Phys. Chem. C* ***125*** 3590-3598.
34. Abidi, W.; Pansu, B.; Krishnaswamy, R.; Beaunier, P.; Remita, H.; Imperor-Clerc, M., 2011 *RSC Adv.* ***1*** 434-439.
35. Wang, S.; Park, S. S.; Buru, C. T.; Lin, H.; Chen, P.-C.; Roth, E. W.; Farha, O. K.; Mirkin, C. A., 2020 *Nat. Commun.* ***11*** 2495.
36. Quan, Z.; Wu, D.; Zhu, J.; Evers, W. H.; Boncella, J. M.; Siebbeles, L. D. A.; Wang, Z.; Navrotsky, A.; Xu, H., 2014 *Proc. Natl. Acad. Sci. U. S. A.* ***111*** 9054-9057.
37. Quan, Z.; Loc, W. S.; Lin, C.; Luo, Z.; Yang, K.; Wang, Y.; Wang, H.; Wang, Z.; Fang, J., 2012 *Nano Lett.* ***12*** 4409-4413.
38. Nagaoka, Y.; Tan, R.; Li, R.; Zhu, H.; Eggert, D.; Wu, Y. A.; Liu, Y.; Wang, Z.; Chen, O., 2018 *Nature* ***561*** 378-382.
39. Hamon, C.; Goldmann, C.; Constantin, D., 2018 *Nanoscale* ***10*** 18362-18369.
40. Schulz, F.; Lokteva, I.; Parak, W. J.; Lehmkühler, F., 2021 *Part. Part. Syst. Charact.* ***38*** 2100087.
41. He, Z.; Jiang, H.-J.; Wu, L.-L.; Liu, J.-W.; Wang, G.; Wang, X.; Wang, J.-L.; Hou, Z.-H.; Chen, G.; Yu, S.-H., 2018 *Angew. Chem. Intl. Ed.* ***57*** 8130-8134.
42. Huang, H.; Li, K.; Chen, Z.; Luo, L.; Gu, Y.; Zhang, D.; Ma, C.; Si, R.; Yang, J.; Peng, Z.; Zeng, J., 2017 *J. Am. Chem. Soc.* ***139*** 8152-8159.
43. Kong, F.; Norouzi Banis, M.; Du, L.; Zhang, L.; Zhang, L.; Li, J.; Doyle-Davis, K.; Liang, J.; Liu, Q.; Yang, X.; Li, R.; Du, C.; Yin, G.; Sun, X., 2019 *J. Mater. Chem. A 7* 24830-24836.
44. Zhu, Y.; Zhu, X.; Bu, L.; Shao, Q.; Li, Y.; Hu, Z.; Chen, C.-T.; Pao, C.-W.; Yang, S.; Huang, X., 2020 *Adv. Funct. Mater.* ***30*** 2004310.
45. Huang, L.; Zhang, X.; Wang, Q.; Han, Y.; Fang, Y.; Dong, S., 2018 *J. Am. Chem. Soc.* ***140*** 1142-1147.
46. Jiang, K.; Zhao, D.; Guo, S.; Zhang, X.; Zhu, X.; Guo, J.; Lu, G.; Huang, X., 2017 *Sci. Adv.* ***3*** e1601705/1-e1601705/8.
47. Liu, Z.; Yin, Y.; Yang, D.; Zhang, C.; Ming, P.; Li, B.; Yang, S., 2020 *RSC Adv.* ***10*** 6287-6296.
48. Gao, H.; Bettscheider, S.; Kraus, T.; Müser, M. H., 2019 *Nano Lett.* ***19*** 6993-6999.
49. Ahmad, I.; Derkink, F.; Boulogne, T.; Bampoulis, P.; Zandvliet, H. J. W.; Khan, H. U.; Jan, R.; Kooij, E. S., 2019 *Beilstein J. Nanotechnol.* ***10*** 696-705.
50. Zheng, Y.; Chen, N.; Wang, C.; Zhang, X.; Liu, Z., 2018 *Nanomaterials* ***8*** 192/1-192/12.
51. Yoshida, T.; Mori, T.; Ueda, I., 1983 *J. Colloid Interface Sci.* ***96*** 39-47.
52. Vargas, J. A.; Petkov, V.; Nouh, E. S. A.; Ramamoorthy, R. K.; Lacroix, L.-M.; Poteau, R.; Viau, G.; Lecante, P.; Arenal, R., 2018 *ACS Nano* ***12*** 9521−9531.

53. Chen, X.; Schröder, J.; Hauschild, S.; Rosenfeldt, S.; Dulle, M.; Förster, S., 2015 *Langmuir **31***.
54. Liao, H.-G.; Zherebetskyy, D.; Xin, H.; Czarnik, C.; Ercius, P.; Elmlund, H.; Pan, M.; Wang, L.-W.; Zheng, H., 2014 *Science **345*** 916-919.
55. Petroski, J. M.; Wang, Z. L.; Green, T. C.; El-Sayed, M. A., 1998 *J. Phys. Chem. B **102*** 3316-3320.
56. Gan, L.; Cui, C.; Heggen, M.; Dionigi, F.; Rudi, S.; Strasser, P., 2014 *Science **346*** 1502-1506.

Figures

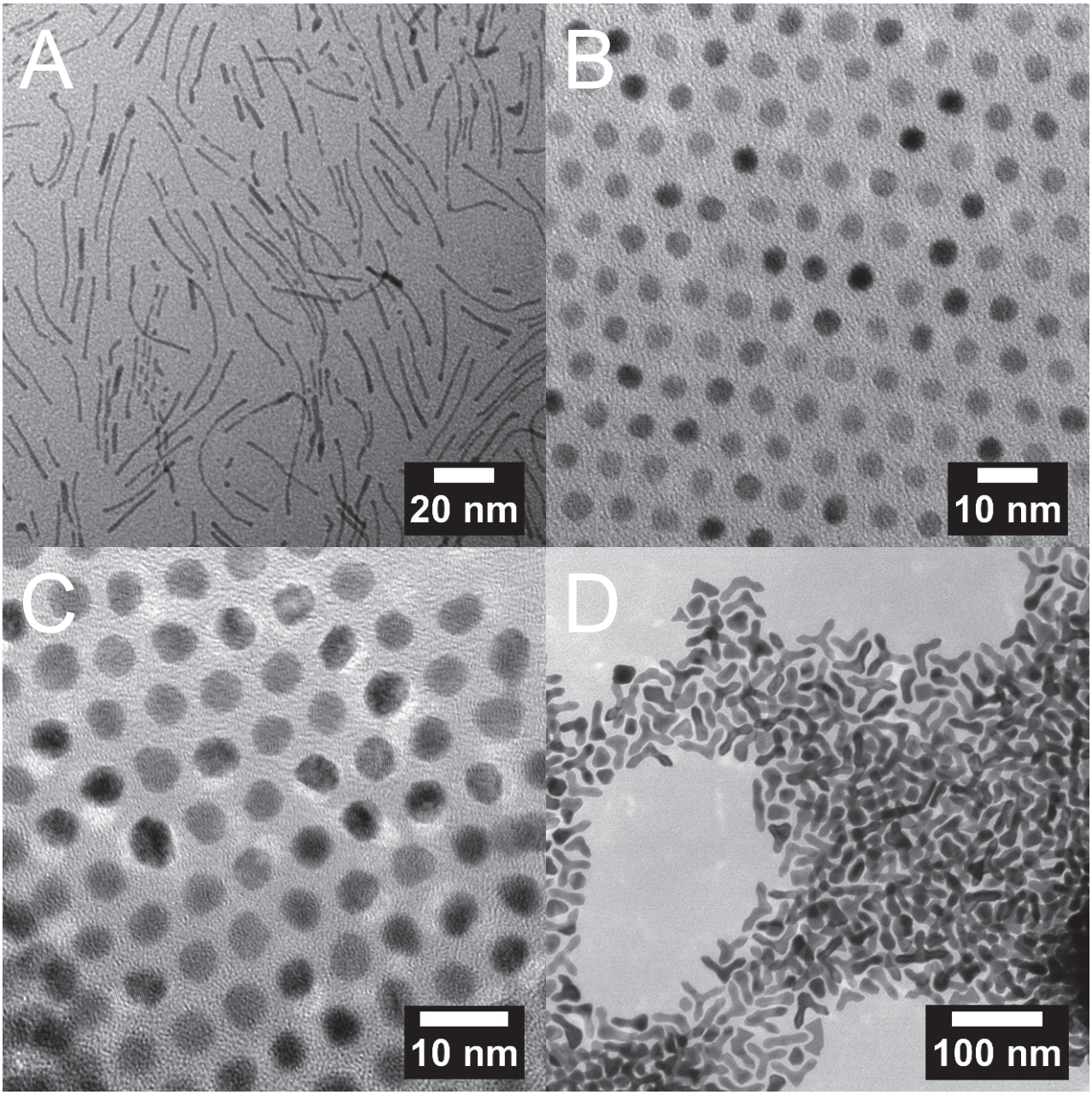

Figure 1. TEM images of samples generated (A) under typical reaction conditions, (B) in the absence of CTAB, (C) in the presence of KBr instead of CTAB, and (D) in the absence of $Mo(CO)_6$, respectively.

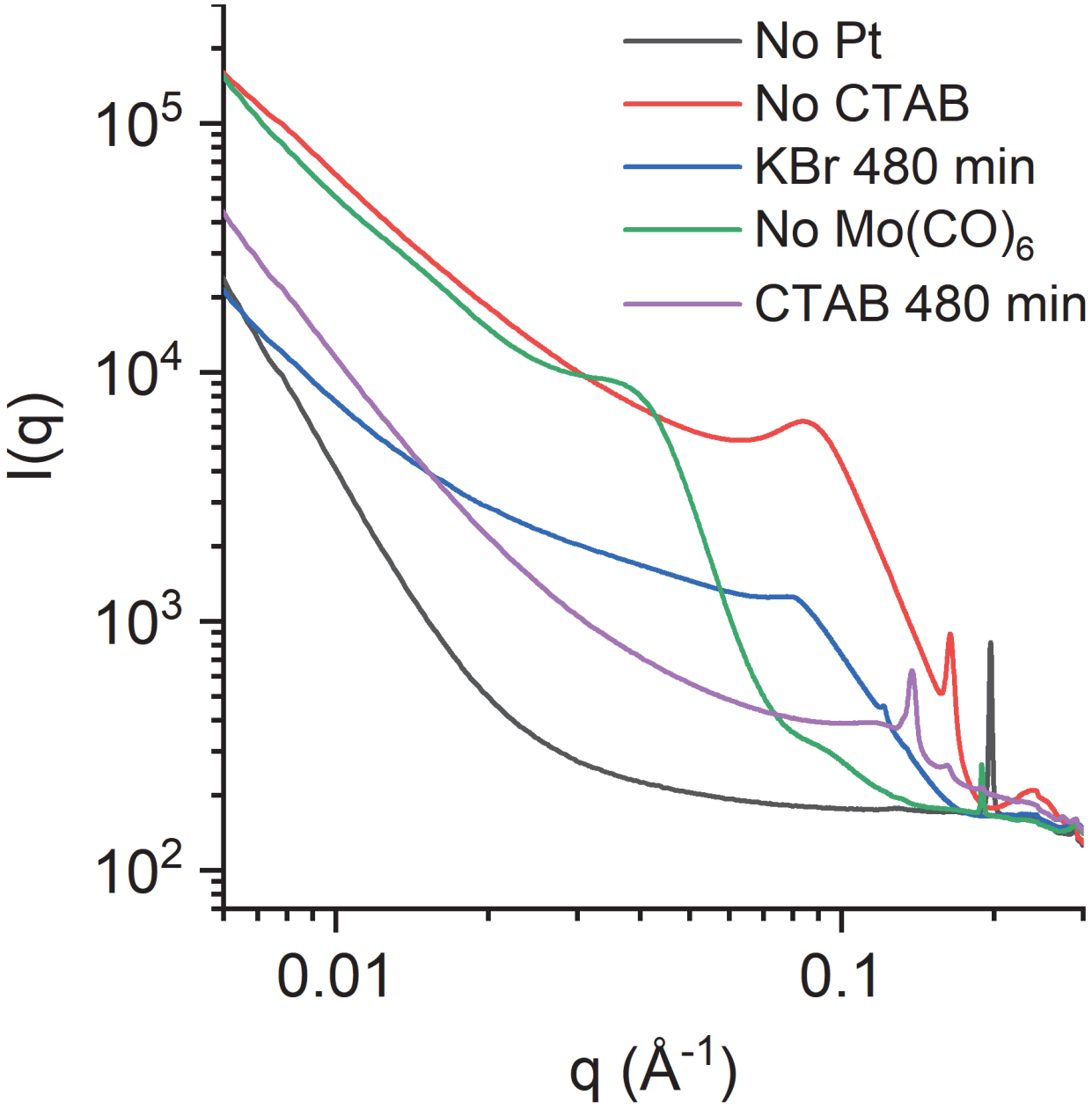

Figure 2. SAXS spectra for samples, synthesized under various reaction conditions, at a set reaction time of 480 min.

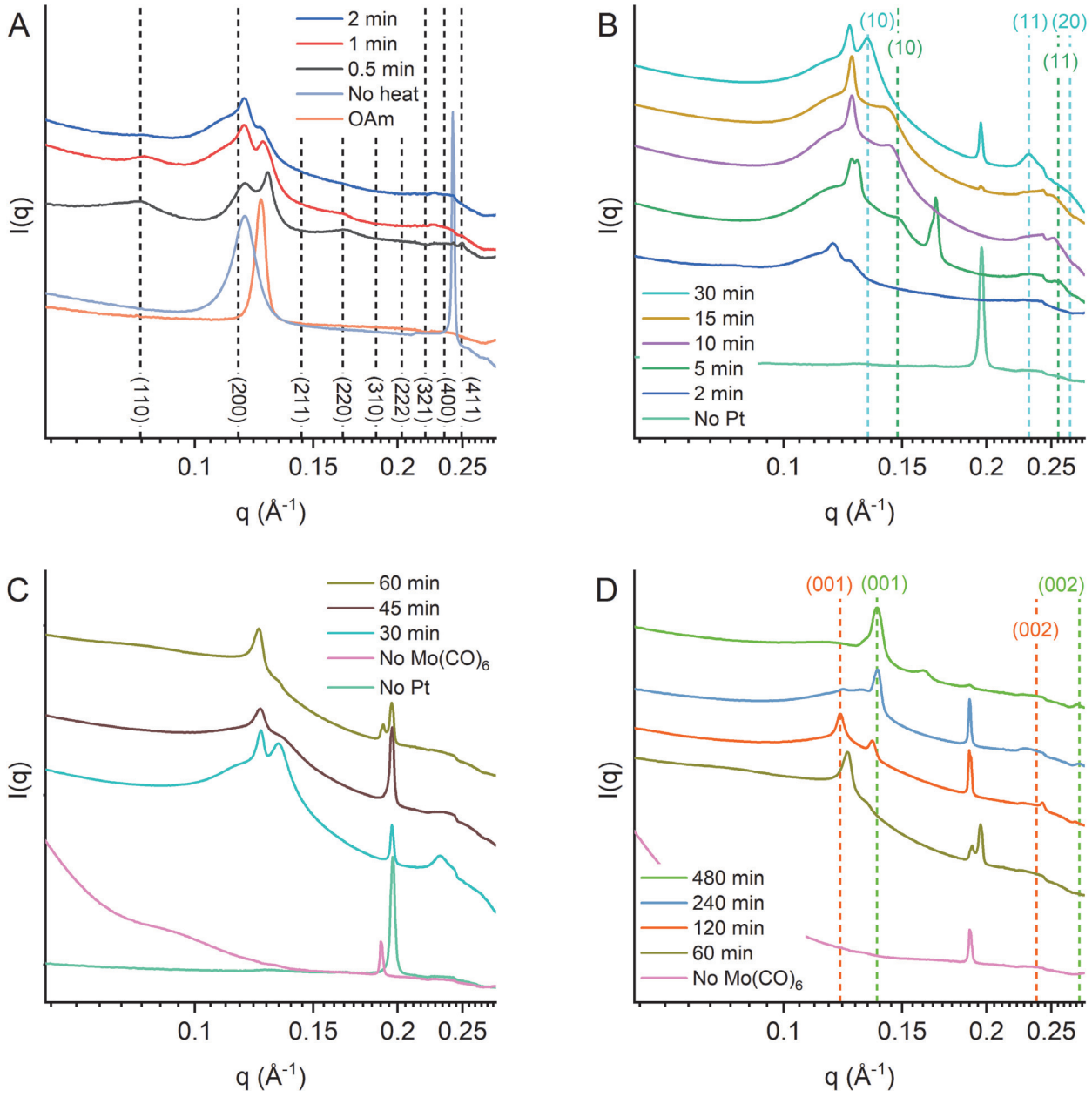

Figure 3. SAXS spectra of samples, prepared at different time intervals. Data were collected at reaction times of (A) 0.5 to 2 min, (B) 2 to 30 min, (C) 30 to 60 min, and (D) 60 to 480 min, respectively.

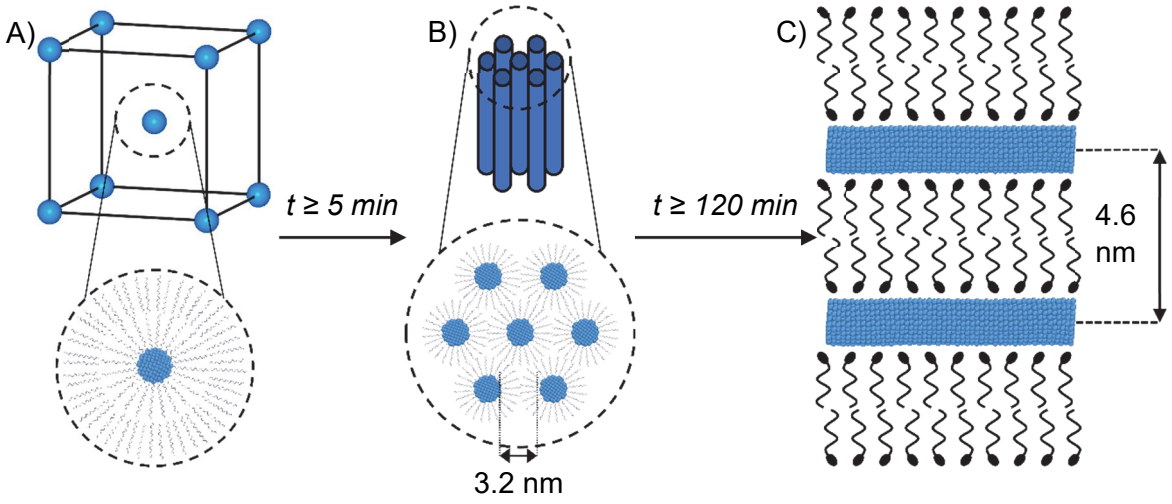

Figure 4. Schematic, depicting the growth and self-assembly mechanism of ultrathin Pt nanowires. (A) Pt nanoparticles initially arranged in a *bcc* superlattice and enveloped within a surfactant bilayer. (B) A hexagonal columnar structure of Pt nanowires, which are coated with a surfactant monolayer. (C) Pt nanowires separated by surfactant-based bilayer lamellae.